Implementations and Evaluations of Wind Turbine Inertial Controls with FAST and Digital Real-Time Simulations

Xiao Wang, David Wenzhong Gao, Senior Member, IEEE, Jianhui Wang, Weihang Yan, Wei Gao, Eduard Muljadi, Fellow, IEEE, Vahan Gevorgian, Senior Member, IEEE

Abstract—This paper presents a novel simulation approach to evaluate new ancillary service controls in the context of largescale wind power integration. We adopt and compare different types of turbine inertial control methods with the proposed modifications to cope with realistic wind conditions in the field. The simulation procedure is started with the software-based simulation, in which we employ the high-fidelity wind turbine simulator FAST that models a real 3-bladed Controls Advanced Research Turbine (CART3). The advantages of using FAST is that it can provide convincing simulation results and address the interactions between turbine electrical and mechanical systems. The developed controller model is then rapidly prototyped for the real-time simulation with the hardware-in-the-loop (HIL) scheme. CART3 will respond to a virtual frequency event triggered in the emulated electric grid modelled in a digital realtime simulator (DRTS). The introduced simulation platform streamlines the procedure of designing turbine auxiliary controls, and these simulations results give insights on the turbine controls and their impacts on the interconnected power system, as well as the effects on turbine mechanical components. For example, the results indicate that the inertial controls tend to reduce the outof-plane mechanical loadings in region 2, while such loadings are dominated by the pitch actions in region 3.

Index Terms—Inertial response, HIL, DRTS, wind power integrations, ancillary service.

I. INTRODUCTION

The worldwide wind energy is experiencing a steady increase in the last few decades. Wind power has represented 33% of all U.S. power capacity additions since 2007, and this percentage is still increasing with the current wind power growth rate [1]. According to the Wind Technology Market Report, the wind power grew at a rate of 12% in 2015 and stands at nearly 74GW, meeting an estimated

5.6% of U.S electricity demands [2]. The increased capacity of individual wind turbine poses challenges on the turbine controls and wind power plants (WPPs) integration. The basic turbine control system should account for the increased turbine structural flexibility through the generator torque and blade pitch control loops, so an efficient energy production with a reduced levelized cost of energy can be achieved [3]. On the other hand, integrating high levels of wind power into an electric grid requires significant changes to power system planning and operations to ensure continued reliability [4]. The testing procedures in international standards (e.g., IEC 61400) should be performed to ensure that the WPP complies with the grid codes in terms of frequency responsive controls and voltage controls [5].

Generally, software-based simulations are the first step to demonstrate the system's ability to provide various types of ancillary services to enhance grid reliability [6], but the results depend largely on the model accuracy, and such softwarebased test might not be adequate. Alternatively, the device under test is connected to a real power system in field testing, however, experiencing the entire range of grid conditions is often not guaranteed [5] for this type of hardware-based testing. Within this context, hardware-in-the-loop (HIL) techniques, combining the testing device and the rest of the system that is simulated in a real-time simulator, are regarded as a cost-effective way with desired flexibility and scalability [7]. The core of a HIL simulation is a digital real-time simulator (DRTS) that is capable of simulating various power system transients or devices dynamics in real time. HIL techniques were firstly used to test relays under several simulated power system abnormal conditions [8], known as a typical controller hardware-in-the-loop (CHIL) application. Recently, this technique receives increased attention due to the research topics on power converter-based energy sources [9]; such simulations can be conducted at full-power levels through the power hardware-in-the-loop (PHIL) technique.

Wind turbine generators (WTGs) are usually represented by the well-known voltage and flux equations in the rotating reference frame. Some research combines this WTG electrical system model, with the mechanical components modelled in a prevalent turbine simulator – FAST (Fatigue, Aerodynamics, Structures, and Turbulences) software package [10]-[14]. References [10] and [11] employ this scheme to model a permanent-magnetic synchronous generator (PMSG)-based

This work is supported in part by the U.S NSF under Grant 1429093 and Grant 1711951.

X. Wang and J. Wang are with the College of Information Science and Engineering, Northeastern University, Shenyang, China. X. Wang was also with the University of Denver.

W. Gao, W. Yan and Wei Gao are with the Department of Electric and Computer Engineering, University of Denver, CO, USA. (wenzhong.gao@du.edu).

Eduard Muljadi is with the Department of Electric and Computer Engineering, Auburn University, AL, USA.

Vahan Gevorgian is with the National Renewable Energy Laboratory, Golden, CO, USA.

^{*}Corresponding author: David Wenzhong Gao

wind turbine, but the variables from turbine mechanical components are not analyzed. The study presented in [12] examines the response of a doubly-fed induction generator (DFIG) to the voltage sags at the point of common coupling (PCC). The results indicate that the voltage fault can cause severe turbine tower vibrations. The authors of [13] show that periodic oscillations in the mechanical system of a fix-speed wind turbine will result in voltage and frequency oscillations in an isolated power grid. Inspired by these research, we employ FAST to model a real three-bladed Controls Advanced Research Turbine (CART3) and use it for turbine inertial response investigations. One of the advantages of using FAST is that the developed controller model can be rapidly thanks to such high-fidelity simulations. References [10]-[13] use FAST to model fictional wind turbines, and these studies are restricted to offline simulations. In this paper, by contrast, the developed control algorithm is deployed in the CART3 real-time controller for the subsequent HIL simulations.

Representative research related to HIL simulations for wind power applications can be found in [15]-[17]. Reference [15] proposes to use a PHIL implementation to investigate the discrete WTG models, and the test bed is also of interest for the verifications of high-level auxiliary WPP controls. Moreover, the WPP controller models, including the frequency control and the oscillation damping functions, are tested utilizing the utility-scale renewable energy test facility at the National Wind Technology Center (NWTC) in Colorado, USA [5], and a 7MW-grid simulator functions to provide designed transient conditions at the PCC. The authors of [16] and [17] illustrate a PHIL test bed using small dynamometers in laboratory environments for turbine control validations. Besides, a unified HIL test bed with two 2.5MWdynamometers and one 5MW-grid simulator is introduced in [18], based on which a novel maximum power point tracking (MPPT) algorithm is verified. However, in these surveyed research either real-time simulated turbine models [15], smallscale [16] [17] or real-scale [18] dynamometers are used, and no real turbines are included in the test beds. The dynamometer is a cost-effective way that uses a motor to emulate aerodynamic torques on a turbine shaft, but the impacts on turbine blades and tower cannot be easily assessed. A real turbine is included in the simulation loop in [5], but auxiliary controllers are not accessible from this commercial turbine and the authors only use the testing results to verify the generic turbine and controller models. Different from these work, the real 600kW CART3 with the prototyped physical controller is included in our HIL simulation loop, with the power grid simulated in a DRTS in real time. In this paper, we concentrate on the turbine inertial response, but other types of auxiliary controls can be effectively evaluated through the introduced test bed as well.

The controlled inertial response of a wind turbine is believed to be more flexible than that of a synchronous generator. The turbine active power output can be shaped in terms of its magnitude and duration through the power converter controls [19], and a substantial amount of kinetic

energy will be released and sustained for tens of seconds. Various inertial control methods are discussed in [19]-[24], with the assumption of a constant wind speed, which is not realistic and will pose difficulties in real applications. For example, the inertial control method by shifting the MPPT curve [23] and the torque-limit-based inertial control (TLIC) [24] require the detection of the quasi steady-state turbine operation point, after which the deloading control is initiated for the turbine to restore its kinetic energy. However, this is not easily achieved as the rotor speed continuously changes in reality under turbulent winds. A more straightforward inertial control scheme coordinated with the actions of a battery energy storage is discussed in [11]. The generator torque is simply commanded at the torque limit during the frequency support. Nevertheless, this might lead to a thermal breakdown of the machine-side converter due to the long-term overproduction. The same issue might also happen to the TLIC method in region 3, when the turbine keeps operating at the torque limit with rated rotor speed.

The aforementioned issues should be solved from a practical perspective for implementations, otherwise the turbine system might be damaged due to the auxiliary inertial controls. In this study, we firstly modify the TLIC method, and employ FAST to simulate and compare it to a commonly used frequency-based inertial control (FBIC) method in the offline simulations. The impacts on the interconnected power grid are analyzed, with an emphasis on the interactions to the turbine mechanical systems. Afterwards, the real-time HIL simulation is carried out using the rapidly prototyped physical controller, with the real CART3 in the simulation loop.

The rest of this paper is organized as follows: Section II introduces the modeling of CART3 and the electrical power grids. The configurations of the HIL simulation platform is illustrated in Section III, with the presented hardware systems. In Section IV, two inertial control methods are presented and to be compared in the offline and real-time simulations in Section V; the paper is finally concluded in Section VI.

II. SOFTWARE-BASED SIMULATION

A. 3-Bladed Controls Advanced Research Turbine (CART3)

CART3, as shown in Fig. 1(a), is a 600kW three-bladed wind turbine operated by the National Renewable Energy Laboratory (NREL). This machine is specially designed for testing advanced control concepts with a customized and reprogrammable real-time controller. CART3 employs the Type 4 WTG configuration with a full power converter system. Numerous sensors are equipped to monitor its performance [25]. Modern turbine control actuations are available on CART3, including the variable-speed controls and the independent blade pitch controls. Detailed CART3 parameters are listed in Table 1.

The wind power coefficient (C_p) surface of CART3 is plotted with respect to the pitch angle and tip-speed ratio (TSR) as shown in Fig. 1(c), which is obtained through a prior simulation and rotor commissioning procedure. The maximum energy conversion efficiency is attained ($C_{p,max}$ =46.58%) when the pitch angle equals 3.7 degree and TSR equals 7.1.

According to the operating regions defined in Fig. 1(b), the generator torque is commanded to the square of measured generator speeds at below-rated wind speeds (region 2) for MPPT operation. The turbine is forced to sit idle in region 1 as there is not enough wind speed to generate power. CART3 employs a gain-scheduling proportional-integral (PI) scheme for the pitch control at above-rated wind speeds in region 3. A transient region 2.5 exists to make the turbine smoothly reach the rated torque in region 3.

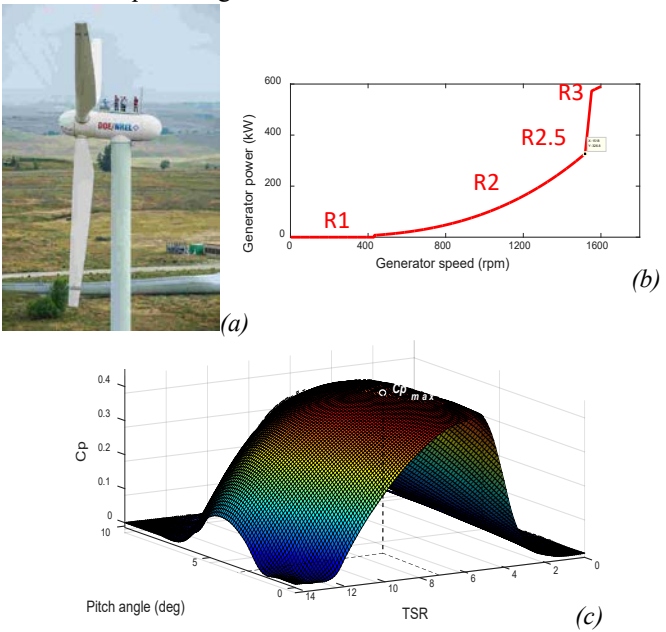


Fig. 1. CART3 and its C_p surface. (a) CART3 (Photo by Lee Jay Fingersh, NREL 24342); (b) CART3 operating regions; (c) CART3 power coefficient surface plotted based on the historical turbine operation data.

Table I CART3 Parameters	
Rotor radius	20 m
Hub height	34.9 m
Drivetrain stiffness coefficient	2.47e ⁷ N-m/rad
Drivetrain damping coefficient	$1.4e^{4} \text{ N-m/s}$
Generator inertia	46 kg.m^2
Hub inertia	3899.7 kg-m^2
Nacelle inertia	36590 kg-m^2
Gearbox ration	43.165
Maximum C_p	0.4658
Optimal TSR	7.1
Minimum pitch angle	3.7 degree
Rated generator torque	3524.37 N-m
Rated generator speed	1600 rpm
Rated rotor speed	41.7 rpm
Rated power output	600 kW

B. CART3 Modeling in the FAST Code

FAST is a sophisticated wind turbine simulator developed by NREL, and it is prevalent in the area of turbine control designs. This program models the turbine blades, tower and shaft as flexible bodies, connected with several degree of freedoms (DOFs); up to 24 DOFs can be switched on to model a 3-bladed turbine in detail [14]. FAST employs Kane's method to set up the equations of motion as given in (1),

 $M(q,u,t)\ddot{q} + f(q,\dot{q},u,u_{\rm d},t) = 0$ (1) and solve it through numerical integrations. M is the mass matrix of all components; f is the nonlinear force function vector; q, \dot{q} , \ddot{q} are the vectors of DOF displacements, velocities and accelerations; u, $u_{\rm d}$, t are controls, disturbances

and time, respectively. Based on the blade element momentum (BEM) theory, the aerodynamic forces of air inflows are calculated by the internal subroutine AeroDyn using 3D wind profiles and airfoil data. These calculated aerodynamic forces are applied in the dynamics of turbine motions in FAST at each time step. However, most research, by contrast, models the wind aerodynamics through the general aerodynamic equations with the mathematically regressed C_p curves [15]-[18] [20]-[24]. The wind speed profiles are generated by the stochastic, full field, turbulent wind simulator TurbSim [26] in the FAST simulations. This provides various designed wind conditions to test the developed controls. Post-processing tools developed by NREL are also available, which helps to analyze FAST simulation results for estimating fatigue and extreme turbine mechanical loadings.

Figure 2(a) shows the diagram of the CART3 model in FAST and the process of developing controller for rapid prototyping. In addition to the drive train and variable-speed generator DOFs, we select the important blade flapwise and edgewise bending DOFs, as well as the tower fore-aft and side-to-side bending DOFs, which have been proven to have important impacts on the turbine operations [27]. As shown in Fig. 2(b), the tower fore-aft and blade flapwise bending are generally known as the out-of-plane loadings, and the tower side-to-side and blade edgewise bending are defined as inplane loadings. Note that when the pitch moves towards feather in region 3, both of the blade flapwise and edgewise bending will contribute to the in-plane and out-of-plane loadings. The advanced control methods are realized in the exportable discrete controller using Simulink as shown in Fig. 2(a). This block is compiled and ported into the CART3 System Control and Data Acquisition (SCADA), through which the control algorithm is downloaded into the National Instrument PXI issuing control commands in real time.

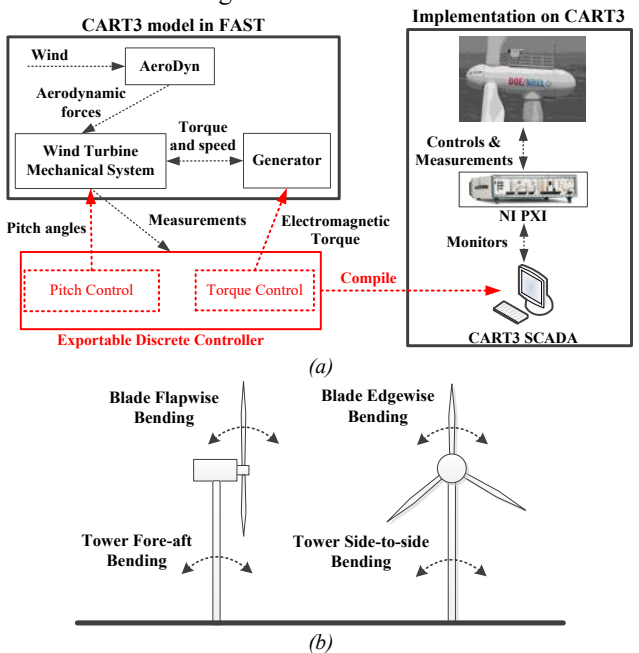


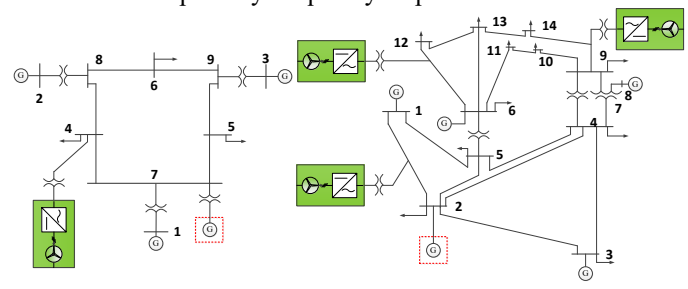
Fig. 2. (a) CART3 simulation model based on the FAST code with the exportable discrete controller built for rapid prototyping; (b) selected DOFs of the turbine tower and blades.

With the detailed turbine mechanical system model, the

PMSG is represented by a simple first-order unit in this study. The power converters are simplified using the three-phase controlled current sources model as mentioned in [28]. The injected active power and reactive power are controlled independently using PI regulators in the direct and quadrature axis. This scheme is also adopted in [29] in order to enhance the real-time computation efficiency of the DRTS.

C. Test Power System Modeling

The electric power systems are modeled by the built-in blocks in SimPowerSystems of MATLAB/Simulink. We adopt two distinct power system topologies, e.g. the WSCC 9-bus grid and the IEEE 14-bus grid as shown in Fig. 3. Detailed parameters for the two test systems can be found in [19] and [30]. One hundred CART3 is aggregated into a WPP represented by each green block with 60WM capacity. The synchronous generators denoted in the red blocks are manually tripped to cause the frequency excursion. The droop coefficient of the speed governor is set to 20%. The automatic generation control (AGC) is also implemented, and we employ a PI controller to assign the power set points of each generator through the grid frequency feedback. The PI controller is tuned to ensure that the response of the AGC is slower enough than that of the primary frequency response.



(a) WSCC 9-bus power system; (b) IEEE 14-bus power system. Fig. 3. Topologies of the test power systems.

III. CONFIGURATIONS AND HARDWARE OF THE REAL-TIME HIL SIMULATION

A. Configuration of the HIL Testing Platform

After the inertial controller model is completely evaluated in the offline simulations, the control algorithm is deployed in the CART3-side PXI and control the turbine in real time. We build the CHIL simulation platform to further evaluate the real turbine's response to the frequency deviation emulated in the DRTS. The offline simulation is an important preliminary to the HIL simulations, and the observations from the real turbine can further support the findings in the offline simulation. The SACAD of CART3 is developed using LabVIEW, so the efficient prototyping relies on the code transformation between MATLAB/Simulink and LabVIEW. As shown in Fig. 4, the CHIL configuration includes the CART3-side controls, monitors, protections (dotted-dashed box on the left), and the RTDS-side real-time simulated power system (dotted-dashed box on the right). These two parts communicate through the SCRAMNet protocol.

In the HIL simulation, we employ the system frequency measurement from the Real-Time Digital Simulator (RTDS) and the CART3 active power measurement to form the closedloop simulation. Figure 4 shows that the frequency deviation is triggered manually in the emulated power system, and this grid frequency signal is sent to CART3. The turbine will respond to this virtual frequency excursion monitored in its SCADA and release the inertial response according to the implemented control algorithms. The active power output at the terminal of CART3 power converters is measured and fed back to the RTDS through the established communication layer. These constitute the entire closed-loop simulation. A three-phase controlled current source reproduces the same amount of CART3 active powers in the emulated grid, assuming that the WPP is operated under unity power factor. Moreover, the RTDS and NREL computers share the same NREL network according to Fig. 4, so real-time simulations can be started remotely via a VPN tunnel, considering that strong winds usually blow during the night.

Note that although the real CART3 is included in the configuration, there is no power loop in this HIL simulation. The signals exchanged between CART3 and the RTDS are at low-voltage, low-power levels, constituting a CHIL simulation to effectively validate the implemented inertial controls. The PHIL test ability will be included in our future studies.

B. Hardware of the Simulation Platform at the CART3 Side and the DRTS Side

Figure 5 (a) shows the hardware at the CART3 side. The

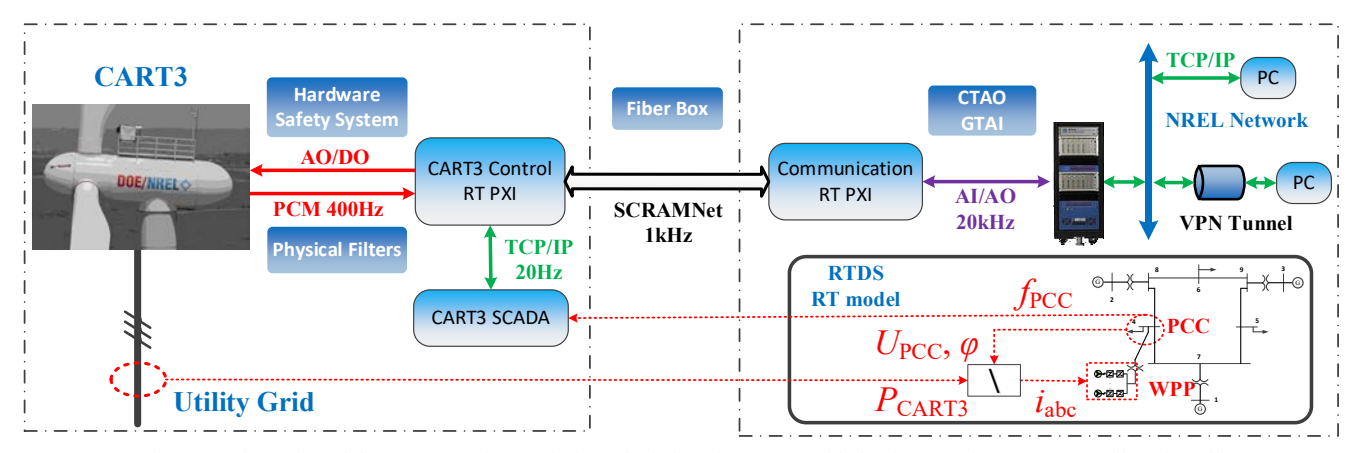
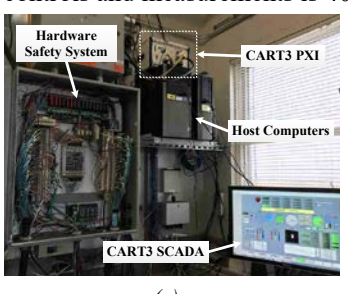


Fig. 4. Configuration of the CHIL simulation platform, including the CART3 side hardware and SCADA, as well as the grid side DRTS and its communication layer.

basic turbine control functions are implemented in the National Instrument PXI controller (PXI-8010) that issues the generator torque and pitch angle commands through the PXI's AI/AO module (PXI-78833R) at each time step. The hardware safety system acts to protect the turbine in case of any malfunctions happening in the turbine controls. In this situation, the protection system will bypass the turbine controls in the PXI and shut down the turbine immediately. Besides, a rotor over-speed protection mechanism is specially implemented in this safety system. The measurement signals from the sensors and strain gages will pass through the physical filter before entering into the PXI. The SCADA, developed in LabVIEW, runs on the host computers and communicates with the PXI via TCP/IP to decide the turbine startup, high-wind cut off, and monitor the performance of each subsystem. The sampling frequency at the CART3-side controls and measurements is 400Hz in the PXI.



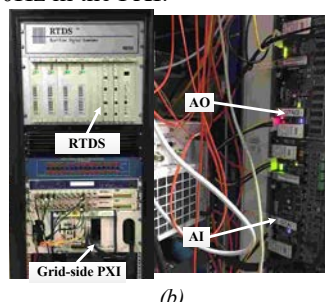


Fig. 5. Hardware pictures of the HIL simulation platform: (a) CART3 side hardware including CART3 real-time controller PXI, SCADA and protection system; (b) hardware at the simulated grid side, including the RTDS and a PXI handling communications between CART3 and RTDS.

On the DRTS side of the CHIL simulation, as shown in Fig. 5 (b), a dedicated PXI (PXI-8119) is mounted at the RTDS rack to handle the data transfer between CART3 and the RTDS. The CART3-side PXI and the virtual grid-side PXI are communicated through the SCRAMNet protocol sampling at 1-kHz. This protocol is believed to be ideal for applications requiring a lot of synchronizations and controls. The CART3-side hardware and the RTDS are separately located on NWTC campus, so a fiber box is involved as a relay point. Analog inputs and outputs are used, so the ports on the GTAI, GTAO cards of the RTDS are wired to the PXI data acquisition module (PXI-6259) for the CART3 measurement feedback.

IV. WIND TURBINE INERTIAL CONTROL ALGORITHMS

A. Frequency-Based Inertial Control

The most commonly used WTG inertial control is called the frequency-based inertial control (FBIC), which emulates the inertial response of a synchronous generator [19]. An active power boost is added in addition to the current MPPT power reference when a frequency dip is detected. This active power increment is calculated based on the grid frequency deviation (known as Droop) and the rate of change of frequency (ROCOF). A combination of these two terms is believed to result in an enhanced inertial response. The low-pass filter is usually added to process the ROCOF term in order to get rid of negative impacts of measurement noises on the turbine shaft, while the high-pass filter might be used in

the droop term, helping the WTG recover to MPPT after the frequency support. We utilize the approach discussed in [21] to determine the scale factors for these two terms, which are adjusted adaptively according to the current rotor speeds; to guarantee reliable turbine operations, turbines operating at higher speeds release more kinetic energy within the WPP.

B. Torque-Limit-Based Inertial Control

The FBIC is already available in commercial wind turbines [31]. Recently, more complicated inertial control methods are developed that manipulate the turbine power reference directly in the WTG speed-power plane, such as the TLIC method.

The TLIC method is capable of maximizing the frequency support by understanding the wind turbine over-production capability [24]. Figure 6 shows the power reference that can be separated by the rotor deceleration stage (A-B-C) and acceleration stage (C-D-E-A) in the turbine speed-power plane. The active power is firstly increased from the predisturbance MPPT point A to B, which corresponds to the point on the torque limit; then the power is decreased along the slope B-C, and the turbine settles at the quasi steady-state point C. The active power reference along the slope is denoted as

$$P_{\rm TLIC} = \frac{P_B(\omega_{\rm g}^*) - P_{\rm mppt}(\omega_{\rm g,min})}{\omega_{\rm g}^* - \omega_{\rm g,min}} \left(\omega_{\rm g} - \omega_{\rm g,min}\right) + P_{\rm mppt}(\omega_{\rm g,min}) \ (2)$$
 with the variables defined in Fig. 6. Secondly, the rotor

with the variables defined in Fig. 6. Secondly, the rotor acceleration starts once the turbine decreases its electric power output stepwise from C to D; later, this power reference is sustained along D-E, until it meets the MPPT curve and recovers to the pre-disturbance value via E-A. Compared to a typical step-wise inertial control method given in [20] (illustrated as A-B'-C'-D'-A), the TLIC benefits from the quasi steady-state turbine settling point C as the power reference decreases gradually to C instead of the sudden output electric power reduction (C' to D'), which prevent causing a severe second frequency dip (SFD). Besides, the turbine might decelerate too fast with the power reference along B'-C', leading to an over-deceleration when the rotor speed falls below the minimum speed limit.

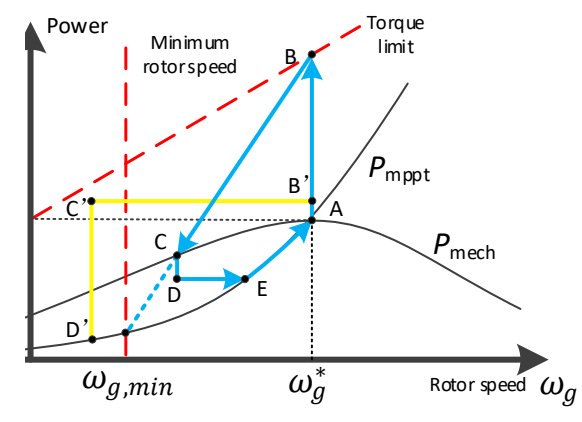


Fig. 6. Power reference of the TLIC illustrated in the turbine speed-power plane: WTG decelerates first through A-B-C, and then accelerates and recovers to the MPPT through D-E-A.

However, wind turbine inertial responses are distinct from that of conventional synchronous generators due to their different topologies and operation manners. Since a turbine has a larger rotor speed operating range, such as a PMSG (speed range from 0.5 p.u. to 1.1 p.u.), the response can be sustained for tens of seconds due to the substantial kinetic energy stored in the rotating mass. Since the response might take longer, ideal and constant wind speed is usually not guaranteed during the course of turbine inertial controls, especially for the TLIC method trying to maximize the frequency support. Reference [23] and [24] proposes to detect the quasi steady-state point C according to the rotor speed changes, which is simply not feasible under wind gusts. Also, the constant power reference along D-E might fail to accelerate the rotor in case of a sudden wind speed decrease.

Furthermore, the turbine operation in region 3 is not considered in [24]. Although the torque limit (assuming 1.2 p.u.) provides extra headroom for the active power increase at the rated condition (rotor speed at 1.0 p.u.), the turbine will get stuck at point B because the turbine cannot be operated along the slope with an invariant rotor speed according to (2). This is because the additional active power boost comes from the extracted aerodynamic power by decreasing the pitch angle, but the kinetic energy stored in the rotating mass is not released. In this situation, the turbine might be overloaded at the torque limit for a long time until wind speed decreases, and such longstanding over-heat is potential to damage the power converters.

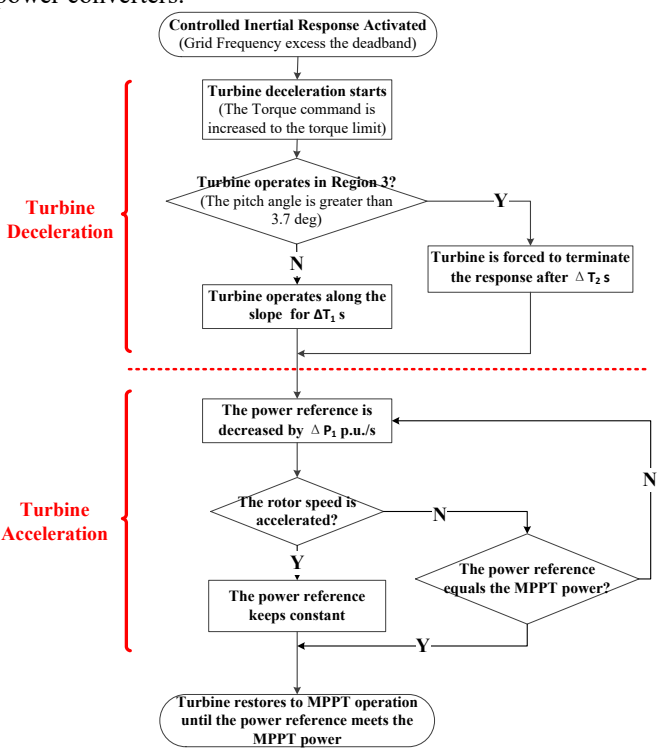


Fig. 7. Flow chart of the modified TLIC method considering the mentioned difficulties in TLIC under wind gusts.

To solve these problems, we modify the TLIC method according to the flow chart shown in Fig. 7. Firstly, instead of detecting the point C, the turbine power reference is set along the slope (B-C) for a predefined duration ΔT_1 . This value is selected to be long enough to guarantee the quasi steady-state operating point is attained, so the SFD can be minimized in the subsequent deloading action. If the turbine is detected to be operating in region 3, the inertial response will be forced to

terminate after ΔT_2 . This value depends on the overproduction capability of the power converters. Secondly, in the rotor kinetic energy restoration stage, the active power is decreased dynamically based on the monitored rotor speed. In order to accelerate the rotor, the power reference keeps decreasing by ΔP_1 /s until rotor speed is measured to increase. This parameter should be carefully designed since an aggressive power decrease may cause a SFD while overdeceleration might happen with a small power decrease rate.

V. SIMULATION RESULTS

A. Offline Simulation Results

Considering the limited capacity of the isolated test grids, we generate wind data with 5% turbulence intensity to prevent unnecessary grid frequency disturbances due to the wind gusts. The mean wind speed values are set to 10m/s (region 2) and 18m/s (region 3) at the turbine hub height. The wind speed profiles are produced by TurbSim with its parameters setting according to the meteorological boundary conditions at the NWTC. We select the simulation results collected in the IEEE 14-bus grid to compare the two inertial controls. The parameters ΔT_1 , ΔT_2 , and ΔP_1 of the modified TLIC is set to 20s, 5s and 0.01 p.u./s, respectively. Note these parameters are scenario-dependent and should be carefully selected. ΔT_1 needs to be long enough to assure that the quasi steady-state point is attained. ΔT_2 should be smaller than ΔT_1 considering the power converters overloading capability in region 3.

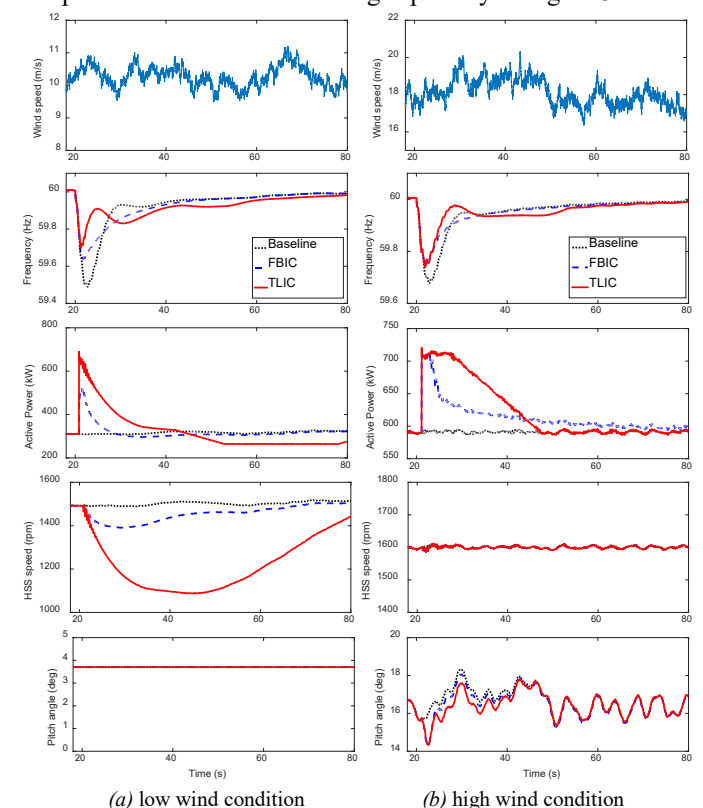


Fig. 8. Simulations results in the IEEE14-bus grid: (a) the scenario at belowrated wind speed; (b) the scenario at above-rated wind speed (black-dotted line: baseline, blue-dashed line: FBIC, red-solid line: modified TLIC).

Figure 8 (a) and (b) show that the controlled inertial response improves the frequency nadir (FN) significantly in

both scenarios with respect to the baseline case that without inertial response. Under the low wind speed condition, the TLIC method improves the FN more than the FBIC, because more active power boost is given at the initial period of the frequency dip. This, consequently, leads to a larger WTG speed decline due to the substantial kinetic energy release, and Fig. 8(a) clearly shows that the inertial response takes effects for tens of seconds until the rotor speed recovers to the predisturbance level. Under the high wind speed condition, the FBIC and TLIC methods have the same amount of active power increase since the turbine is already operating at the rated condition before the disturbance, and this results in a similar FN and ROCOF in the grid frequency profile.

Furthermore, the FBIC method is based on the grid frequency feedback, which contributes to a smooth grid frequency rebound as shown in Fig. 8 (a) and (b), and this might also relate to its damping effect as discussed in [20]. For the TLIC, the grid frequency profile is not as smooth, and SFD may happen during the kinetic energy restoration stage as shown in Fig. 8 (a), whereas such SFD has been mitigated in the proposed TLIC method due to the quasi steady-state point that the turbine settled upon and the moderate active power decrease in the deloading action.

In region 3, the active power increase comes from the aerodynamic power in the wind, therefore, the generator speed keeps constant at the rated value as expected according to Fig. 8 (b). The turbine begins to decrease its active power from the torque limit after around 5 seconds as specified in the modified TLIC method, which also leads to a smaller pitch angle compared to the baseline and the FBIC method, because more aerodynamic power needs to be extracted to compensate for the larger energy release. These results indicate that a turbine operating in region 3 can contribute to grid frequency regulations with appropriate designed headroom, and such inertial response will not sacrifice the stored kinetic energy, but the turbine overproduction, in terms of its strength and duration, should be carefully considered before deployment.

In addition, the important turbine mechanical loadings, including the blade flapwise and edgewise bending, and the tower fore-aft and side-to-side bending, are analyzed based on the FAST outputs. These interested loadings are illustrated in Fig. 2(b). Figure 9 shows that the blade and tower bending moments undergo periodic oscillations due to the turbine rotation and the impacts from external environment, such as wind shears and gravity. Also, the turbine pitch and torque controls have important influence these mechanical loadings. In region 2, it is obvious from Fig. 9(a) that the tower fore-aft bending is reduced by the inertial response with the TLIC method. The blade flapwise bending also shows decrease but not as obvious as the tower fore-aft bending. The blade flapwise and tower fore-aft bending are generally perpendicular to the rotor plane and known as the out-of-plane turbine loadings. The inertial response tends to reduce the outof-plane turbine loadings, which are primarily determined by the thrust from the wind. Such thrust-coupled loadings [25] will be reduced as the turbine is operated in the quasi steadystate status, so the aerodynamic force acting on the rotor disk

is decreased. The blade edgewise bending, related to the inplane loading, is dominated by the cyclic gravitational loading, which will increase with greater rotor speed [25]. The results presented in Fig. 9(a) does not show a clear increase or decrease in blade edgewise bending, and this might be because the inertial response changes the rotor speed not as much as the turbine primary frequency regulation; the blade edgewise bending will increase when the rotor is over speed for power reserves as discussed in [25]. Another observation is that the magnitude of tower side-to-side bending is increased during the inertial response.

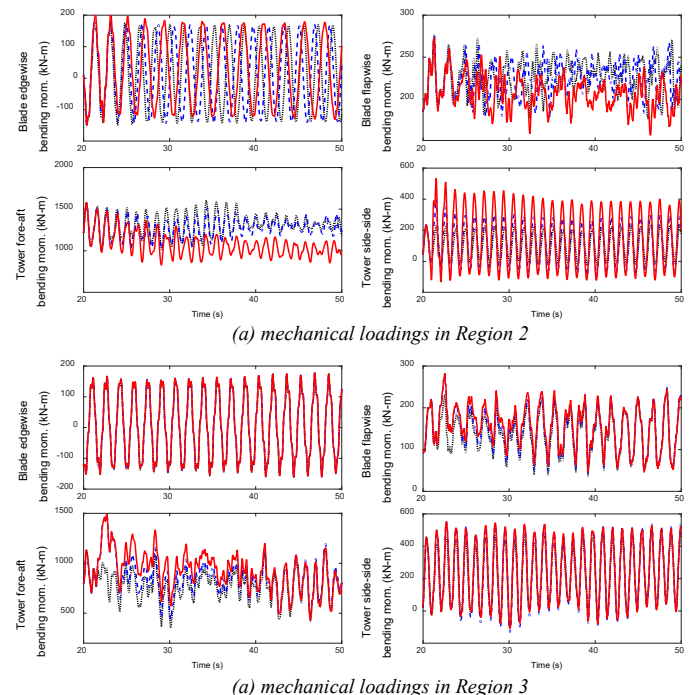


Fig. 9. CART3 blade and tower mechanical loadings under the low wind speed condition (black-dotted line: baseline; blue-dashed line: FBIC; red-solid line: TLIC).

In region 3, the trends of increased or decreased loadings are distinct from that shown in region 2. The only clear observation is that the TLIC method holds the highest tower fore-aft bending as shown in Fig. 9(b). This is reasonable because the TLIC method has the lowest pitch angle during the inertial response, and in region 3, such out-of-plane loadings will be dominated by the pitch actuation. The blade flapwise bending does not show similar trend as the tower fore-aft bending as that in region 2, because the blade flapwise bending will also contribute to the in-plane loadings when the pitch rotates towards feather in region 3, and this applies to the blade edgewise bending as well. From our previous studies [19], the inertial response will lead to a load increase on the turbine shaft due to an excessive generator torque extraction. It shows that a torque rate limiter is beneficial to alleviate the negative influence on the turbine shaft, although the strength of inertial response is mitigated accordingly [19].

B. CHIL Simulation Results

The evaluated inertial control algorithms are implemented in CART3 for the following CHIL simulations. The WSCC 9-bus system is adopted as the emulated grid. We first compare

the CART3 active power and their impacts on the power grid frequency. The simulation results obtained under similar wind conditions are selected as shown in Fig. 10(a) and (b). The turbine can increase its active power up to three times of the pre-disturbance values. In general, the TLIC releases a stronger inertial response during the frequency dip, resulting in an improved FN and ROCOF. The improvement on grid frequency is not as obvious as that presented in the offline simulation. This is mainly related to the slightly slow CART3 active power boost in reality, because of the communication delays, the implemented filter and the torque-rate limiter used to protect the real turbine in its control system. Figure 10 (a) also shows that the TLIC method controls the turbine operating at the steady state with the suboptimal power coefficient for the specified time period.

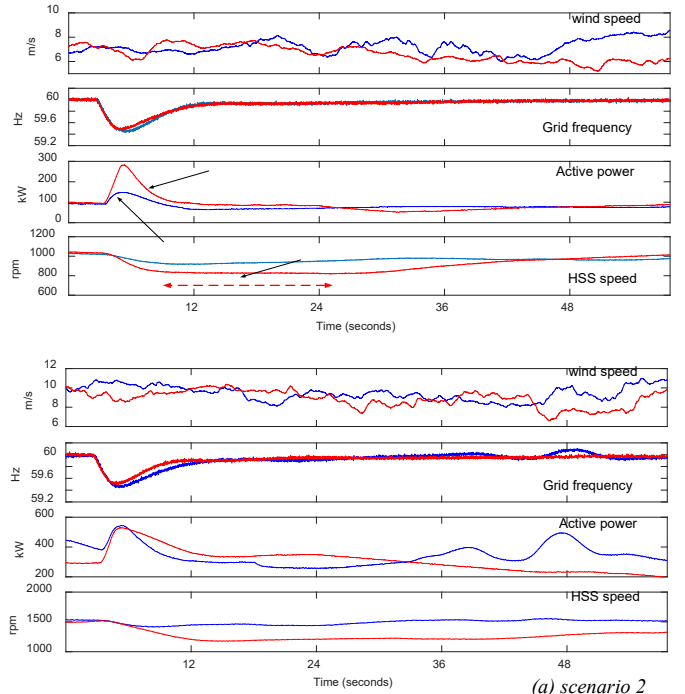


Fig. 10. CART3 active power and generator speed measurements with respect to the grid frequency changes collected in the HIL simulations.

Furthermore, the simulation results of the modified TLIC in region 2 and region 3 are collected and shown in Fig. 11, in which we focus more on the response of the turbine mechanical system. The generator electromagnetic torques (denoted in negative sign) are increased to the torque limit, which yields the obvious CART3 active power boosts both in Fig. 11 (a) and (b). Compared to the results given in Fig. 8, the generator torque and active power increases are less aggressive on the real turbine, and it takes almost 3 seconds to command the generator torque to the limit as indicated in Fig. 11(a). Fig. 11 (a) also shows a slight decrease in the blade 1 flapwise bending in region 2, with no obvious changes in the magnitude of blade 1 edgewise bending. These observations on loads are consistent to the offline simulation results in Fig. 9(a). Figure 11 (b) shows that CART3 finishes its frequency support after nearly 5 seconds in region 3 as specified in the implemented inertial controller. The pitch angle is decreased as expected during the inertial response due to the increased active power output. The blade flapwise and edgewise

loadings do not show clear trends in Fig. 11(b), as the turbine loadings are complicated and combined effects of the turbine pitch control and torque control loops in this operation region. The increased shaft loadings as denoted in the high-speed shaft (HSS) side indicate the negative impacts of turbine inertial controls, but its long-term effects need to be further investigated considering the possibility of providing such control actions.

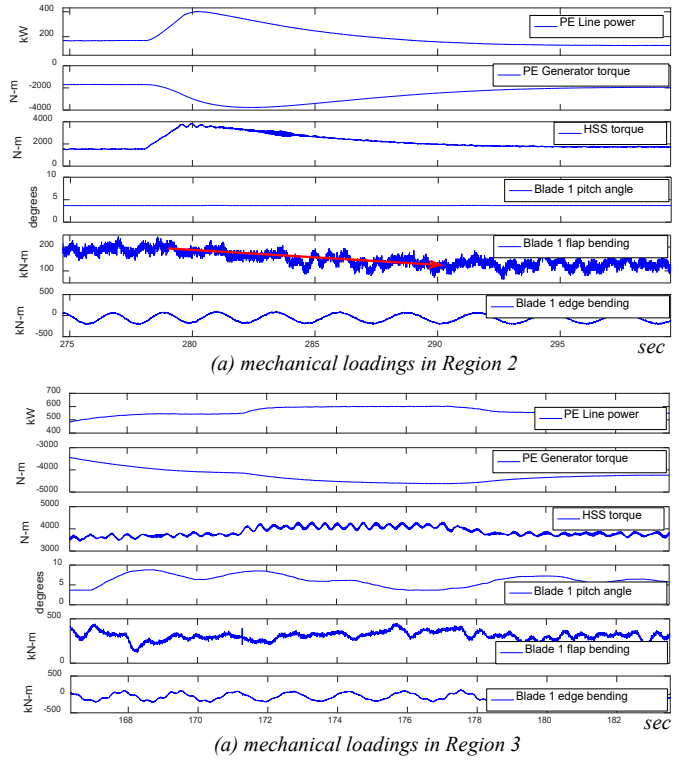


Fig. 11. CART3 generator torque, HSS torque, blade 1 pitch angle and flap bending and edge bending collected in the modified TLIC method.

VI. CONCLUSION AND FUTURE WORK

The controlled inertial response of the WTG is investigated in this work. A novel two-stage simulation approach that combines the offline simulation and the real-time HIL simulations is proposed to evaluate different turbine auxiliary controls. The inertial control algorithms are assessed in the software-based simulation first. The impacts of the inertial responses on the power grid frequency transients and the physical loadings imposed on the turbine mechanical components are evaluated. Once the predicted results from the offline simulations are satisfied, we then implement the controls on the real CART3 and simulate in real-time with the emulated grid in a DRTS. The advantages of using the FASTbased CART3 model is that the developed controller model can be rapidly prototyped and field tested. The results from field testing can be used to further validate the simulation results and improve the implemented control concepts. Note that the value of this work is not restricted only to the turbine inertial controls tested in this paper, but the principle and methodology in realizing such simulation platform can be used in validating other auxiliary controls.

A novelty of this paper is that the real turbine is included in the real-time simulation, but there is no power exchange between CART3 and the emulated grid. NREL has an extensive facility to test various cases on a real turbine, and we propose to use the 7MVA Controllable Grid Interface (CGI) for the PHIL simulation to improve the simulation capability of the advanced simulation platform. Such PHIL simulation platform can be built according to the diagram given in Fig. 12. Additional efforts are required to make connections between CART3 and CGI at full-power levels, considering that certain types of WTGs under test might produce currents up to ten times higher than its nominal rating under abnormal conditions for short time periods. This full-power simulation capability will be included in our future work.

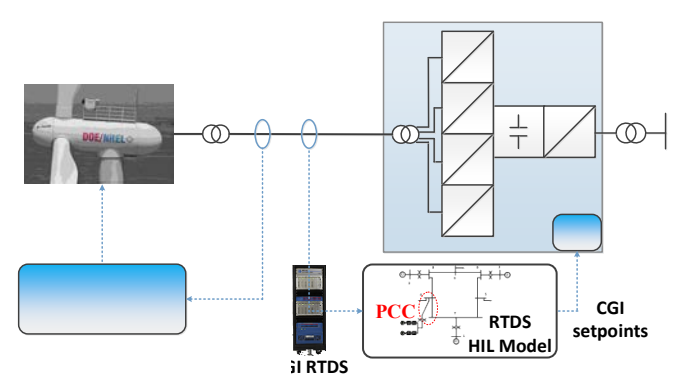


Fig. 12. The diagram of a PHIL simulation platform for our future studies.

VII. ACKNOWLEDGMENT

The authors sincerely acknowledge the contributions from NREL researchers and engineers: Andrew Scholbrock, Paul Fleming, Robb Wallen, and Jason Jonkman for his guidance on the FAST program.

VIII. REFERENCES

- Wind Energy Benefits, Energy Efficiency and Renewable Energy, (U. S Department of Energy).
- [2] R. Wiser, M. Bolinger, G. Barbose, et al., "2015 Wind Technology Market Report," Technical Report, U.S. Department of Energy, 2016.
- [3] A. Scholbrock, P. Fleming, A. Wright, et al., "Lidar-Enhanced Wind Turbine Control: Past, Present and Future," NREL, Golden, CO, Tech. Rep. NREL/CP-5000-65879.
- [4] V. Gevorgian, P. Koralewicz, R. Wallen, et al., "Controllable Grid Interface for Testing Ancillary Service Controls and Fault Performance of Utility-Scale Wind Power Generation," NREL, Golden, CO, Tech. Rep. NREL/CP-5D00-67247.
- [5] L. Zeni, V. Gevorgian, R. Wallen, et al., "Utilisation of real-scale renewable energy test facility for validation of generic wind turbine and wind power plant controller models," in *IET Renewable Power Generation*, vol. 10, no. 8, pp. 1123-1131, Sep. 2016.
- [6] K. Strunz, E. Carlson, "Nested Fast and Simultaneous Solution for Time-Domain Simulation of Integrative Power-Electric and Electronic Systems" in *IEEE Trans. on Power Deliver*, vol. 22, no. 1, pp. 277-287.
- [7] B. Lundstrom, "An Advanced Platform for Development and Evaluation of Grid Interconnection Systems Using Hardware-In-the-Loop," M.S. thesis, Dept. Electron. Eng. and Computer Science, Colorado School of Mines, Colorado, USA, 2013.
- [8] M. D. Omar Faruque, T. Strasser, G. Lauss, et al., "Real-Time Simulation Technologies for Power Systems Design, Testing, and Analysis," in *IEEE Power and Energy Technology Systems Journal*, vol. 2, no. 2, pp. 63-73, June 2015.

- [9] X. Guillaud, M. O. Faruque, A. Teninge, et al., "Applications of Real-Time Simulation Technologies in Power and Energy Systems," in IEEE Power and Energy Tech. Systems Journal, vol. 2, no. 3, pp. 103-115.
- [10] D. S. Ochs, R. D. Miller and W. N. White, "Simulation of Electromechanical Interactions of Permanent-Magnet Direct-Drive Wind Turbines Using the FAST Aeroelastic Simulator," in *IEEE Trans. on Sustainable Energy*, vol. 5, no. 1, pp. 2-9.
- [11] Z. Wu, D. W. Gao, H. Zhang, et al., "Coordinated Control Strategy of Battery Energy Storage System and PMSG-WTG to Enhance System Frequency Regulation Capability," in *IEEE Trans. on Sustainable Energy*, vol. 8, no. 3, pp. 1330-1343.
- [12] R. Fadaeinedjad, M. Moallem, G. Moschopoulos, "Simulation of a Wind Turbine with Doubly Fed Induction Generator by FAST and Simulink," in *IEEE Trans. on Energy Conversion*, vol. 23, no. 2, pp. 690-700.
- [13] R. Fadaeinedjad, G. Moschopoulos, M. Moallem, "The Impact of Tower Shadow, Yaw Error, and Wind Shears on Power Quality in a Wind– Diesel System," in *IEEE Trans. on Energy Conversion*, vol. 24, no. 1, pp. 102-111.
- [14] J. M. Jonkman, L. J. Buhl, "FAST User's Guide," NREL/EL-500-38230. Tech. Report, NREL, 2005.
- [15] F. Huerta, R. L. Tello and M. Prodanovic, "Real-Time Power-Hardware-in-the-Loop Implementation of Variable-Speed Wind Turbines," in IEEE Trans. on Industrial Electronics, vol. 64, no. 3, pp. 1893-1904.
- [16] Y. Zhou, J. Lin, Y. Song, et al., "A Power Hardware-in-the-loop Based Testing Bed for Auxiliary Active Power Control of Wind Power Plants," in *Electric Power Systems Research*, vol. 2015, no. 124, pp. 10-17.
- [17] I. Munteanu, A. I. Bratcu, S. Bacha, et al, "Hardware-in-the-Loop-based Simulator for a Class of Variable-speed Wind Energy Conversion Systems: Design and Performance Assessment" in *IEEE Trans. on Energy Conversion*, vol. 25, no. 2, pp. 564-576.
- [18] H. Li, M. Steurer, K. Shi, et al, "Development of a Unified Design, Test, and Research Platform for Wind Energy Systems Based on Hardwarein-the-Loop Real Rime Simulation", in *IEEE Trans. on Industrial Electronics*, vol. 53, no. 4, pp. 1144-1151.
- [19] X. Wang, W. Gao, A. Scholbrock, et al., "Evaluation of the Inertial Response of Variable-Speed Wind Turbines Simulated by FAST," in IET Renewable Power Generation, vol. 11, no. 12, pp. 1534-1544.
- [20] S. El Itani, U. D. Annakkage and G. Joos, "Short-Term Frequency Support Utilizing Inertial Response of DFIG Wind Turbines," 2011 IEEE PES. General Meeting, San Diego, CA, 2011, pp. 1-8.
- [21] J. Lee, E. Muljadi, P. Sorensen, et al, "Releasable Kinetic Energy-Based Inertial Control of a DFIG Wind Power Plant," in *IEEE Trans. on Sustainable Energy*, vol. 11, no. 12, pp. 279-288.
- [22] M. Hwang, E. Muljadi, G. Jang, Y. C. Kang, "Disturbance-Adaptive Short-Term Frequency Support of a DFIG Associated with the Variable Gain Based on the ROCOF and Rotor Speed," in *IEEE Trans. on Power Systems*, vol. 32, no. 33, pp.1873-1811.
- [23] M. Kang, E. Muljadi, K. Hur, et al, "Stable Adaptive Inertial Control of a Doubly-Fed Induction Generator" in *IEEE Trans. on Smart Grid*, vol. 7, no. 6, pp. 2971-2979.
- [24] M. Kang, K. Kim, E. Muljadi, et al., "Frequency Control Support of a Doubly-Fed Induction Generator Based on the Torque Limit," in *IEEE Trans. on Power Systems*, vol. 31, no. 6, pp. 4575-4583.
- [25] P. A. Fleming, J. Aho, A. Buckspan, et al., "Effects of Power Reserve Control on Wind Turbine Structural Loading," in Wind Energy, vol. 19, no. 3, pp. 453-469.
- [26] B. J. Jonkman, L. J. Buhl, "TurbSim User's Guide," NREL/TP-500-41136. Technical Report, NREL, 2007.
- [27] A. D. Wright. "Modern Control Design for Flexible Wind Turbines," NREL/TP-500-35816. Technical Report, NREL, 2004.
- [28] M. Singh and S. Santoso, "Dynamic Models for Wind Turbines and Wind Power Plants," NREL, Golden, CO, Tech. Rep. NREL/SR-5500-52780, Oct. 2011.
- [29] J. H. Jeon, J. Y. Kim, S. K. Kim, et al., "Development of Hardware Inthe-Loop Simulation System for Testing Operation and Control Functions of Microgrid," in *IEEE Trans. on Power Electronics*, vol. 25, no. 12, pp. 2919-2929.
- [30] S. M. Kodsi, C. A. Canizares, "Modeling and Simulation of IEEE 14 Bus System with FACTs Controllers," University of Waterloo, Canada, Technical Report, 2003.

[31] N. Miller, C. Loutan, M. Shao and K. Clark, "Emergency Response: U.S. System Frequency with High Wind Penetration," in *IEEE Power and Energy Magazine*, vol. 11, no. 6, pp.63-71, Nov.-Dec. 2013.



Xiao Wang received his B.S degree in Automation from the College of Information Science and Engineering, Northeastern University, China in 2013, where he is pursuing the Ph.D. degree in control theory and engineering. From September 2015 to September 2017, he

visited University of Denver as a joint Ph.D. student sponsored by the China Scholarship Council (CSC). He also worked as a research intern at the National Wind Technology Center of National Renewable Energy Laboratory (NREL), Golden, USA. His research interests include applications of advanced controls in wind turbine systems and integrations of large-scale wind power in power grids.



David Wenzhong Gao (S'00–M'02–SM'03) received his M.S. and Ph.D. degrees in electrical and computer engineering, specializing in electric power engineering, from Georgia Institute of Technology, Atlanta, USA, in 1999 and 2002, respectively. He is now with the Department of Electrical and Computer Engineering, University of

Denver, Colorado, USA. His current teaching and research interests include renewable energy and distributed generation, microgrid, smart grid, power system protection, power electronics applications in power systems, power system modeling and simulation, and hybrid electric propulsion systems. He is an Associate Editor for IEEE Journal of Emerging and Selected Topics in Power Electronics. He was an editor of *IEEE Transactions on Sustainable Energy*. He is the General Chair for the 48th North American Power Symposium (NAPS 2016) and the IEEE Symposium on Power Electronics and Machines in Wind Applications (PEMWA 2012).



Jianhui Wang was born in Liaoning Province, China, in 1957. She received her B.S., M.S., and Ph.D. degrees in Electrical Engineering from Northeastern University, China, in 1982, 1986, and 1999, respectively. Her research interests include complex industrial process modeling, control and optimization,

rehabilitation robot, intelligent control and so on. Now, she is full professor and doctoral supervisor at School of Information Science and Engineering, Northeastern University, Shenyang, Liaoning, China. Her current research interests include intelligent control theory and its application.



Weihang Yan received B.S. degree and M.S. degree in Automation from Northeastern University, Shenyang, China, in 2014, and 2016, respectively. Currently, he is pursuing the Ph.D. degree in Electrical and Computer Engineering at

University of Denver, CO. USA. His research interests are applications of power electronics in microgrid, distributed generation technology, and renewable energy integration.



Wei Gao received the Bachelor's Degree in Automation from Hebei University of Technology, Tianjin, China, in 2017. He is studying in the Department of Electrical and Computer Engineering for his Ph.D. degree at the University of Denver, Denver,

Colorado. His research interests are in the area of microgrid control, renewable energy, power system stability.



Eduard Muljadi (M'82, SM'94, F'10) received his Ph.D. in electrical engineering from the Univ. of Wisconsin, Madison. He was a faculty at the California State University, Fresno (1988-1992). From 1992-2017, he worked at the National Renewable Energy Laboratory in Golden, CO. And, in

January 2018, he joined Auburn University in Auburn, AL, as the James J. Danaher distinguished professor. His research interests include electric machines, power electronics, and power systems, and renewable energy. He is a member of Eta Kappa Nu, Sigma Xi, a fellow of the IEEE, and an editor of the IEEE Transactions on Energy Conversion. He is member of various subcommittees within the IEEE Industry Application Society (IAS), Power Electronics Society, and Power and Energy Society (PES). He is currently the chair of Renewable Energy Machines and Systems and the chair of the Future Advanced Pumped Storage Modeling Task Force within the PES. He holds patents in power conversion for renewable energy.



Vahan Gevorgian (M'97) graduated with B.S. and M.S. from the Yerevan Polytechnic Institute in Armenia. He obtained his Ph.D. in electrical engineering from the State Engineering University of Armenia in 1993. Dr. Gevorgian is a Chief Engineer at the National Wind Technology Center of the National Renewable Energy Laboratory in

Golden, Colorado. He is currently focusing on renewable energy impacts on transmission and interconnection issues and dynamic modeling of variable generation systems. He is member of the IEC team for wind turbine power quality standards.